iDim: Practical Implementation of Index Modulation for LiFi Dimming

Trang Nguyen [ID], Mohamed Sufyan Islim [ID], Cheng Chen [ID], and Harald Haas [ID], *Fellow, IEEE*

Abstract—This paper introduces a novel dimming method for Light Fidelity (LiFi) based on a time-domain sample index modulation (TIM), called indexed dimming (iDim). The aim is to provide a wide brightness range, while maintaining a high signal-to-noise ratio (SNR) performance and a high transmission rate. Direct current optical orthogonal frequency division multiplexing (DCO-OFDM) is used and novel line codes are presented. The system performance is experimentally validated by an implementation on a NI PXIe-1085 and NI-7966R Field Programmable Gate Array (FPGA). Implementation results show that the proposed iDim jointly offers multiple benefits compared to existing dimming methods such as amplitude modulation (AM) dimming. Specially, the lowest optical power of the iDim method is measured at 20 μW, which is 10 times lower than the measured limit of AM dimming. The iDim system provides a SNR of 22.5 dB for all brightness levels, while the AM-dimming method dramatically reduces its SNR when light is dimmed. The transmission rate of iDim is also higher than DCO-OFDM. This results in up to 40% reduced optical power per bit when compared to sDim, a pulse-width-modulation (PWM)-inspired dimming method. Therefore, iDim is a promising dimming method for applications targeting extremely low illumination levels.

Index Terms—LiFi, time index modulation, indexed dimming, iDim, line coding, DCO-OFDM.

I. INTRODUCTION

WE ARE currently witnessing the commercial roll-out of fifth generation (5G) mobile networks. Recently, the 6 GHz band was approved for unlicensed WiFi use in the United States of America by the Federal Communications Commission (FCC) in an aim to meet the exponential growth of the wireless traffic. Moreover, a number of emerging technologies are now being considered for the next wireless generation to future-proof the ever-growing bandwidth demand [1]. Light Fidelity (LiFi) is a promising candidate that has matured after more than two decades of development. The light spectrum is interference-free to the entire radio

The authors are with the Department of Electronic and Electrical Engineering, LiFi Research and Development Centre, Technology and Innovation Centre, University of Strathclyde, Glasgow G1 1RD, U.K. (e-mail: trang.nguyen@strath.ac.uk; m.islim@strath.ac.uk; c.chen@strath.ac.uk; harald.haas@strath.ac.uk).

frequency band and considered to be a green solution to meet the requirements of energy efficient networks [2].

LiFi aims to use the existing lighting infrastructure for data communications, thus a LiFi light source can serve both illumination and communication purposes. Several technical and functional requirements, such as flicker-free illumination and dimming, are included in both existing and ongoing light communication (LC) standards [3], [4]. The term 'dimming' in LC standards refers to the ability of a LiFi system to adjust the transmitter brightness during communication. Dimming is required for LiFi scenarios such as (i) indoor lighting that needs brightness control for user convenience, (ii) aircraft LiFi, in which dimmed light is strictly required during flight, and (iii) vehicular laser-based LiFi, in which long-range communication (typically over 100 meters) is mandatory while the optical power is restricted by eye safety regulations.

Establishing high performance communication links at low optical power levels is a desired element of this dimming ability. Several dimming methods are available to use. The existing IEEE 802.15.7-2011 standard [3] proposes pulse-width-modulation (PWM) dimming and amplitude-modulation (AM) dimming methods for rectangular-shaped signals. However, when applying AM dimming and PWM dimming methods to LiFi waveforms, they have shown a degraded performance and a narrow brightness dimming range [5]. Particularly when the transmitter controls the brightness level (% unit), the AM dimming has significant drawbacks in terms of signal-to-noise ratio (SNR) when the light is dimmed. Similarly, PWM dimming also has limitations in terms of the lowest brightness that it can enable, which was measured at 16% [5]. Moreover, the transmission of any LiFi waveform requires a certain offset voltage to avoid signal distortion and clipping. In a LiFi dimming scenario, this results in a minimum optical power that is defined as a 0% brightness level. However, the 0% brightness level depends on the selection of the bias voltage. Thus, even if a dimming level at 0% brightness is used, the LiFi transmitter will not be entirely off. This limitation can be solved by a novel temporal index modulation (TIM) dimming method, termed indexed dimming (iDim). The iDim scheme is applied to a direct current (DC) optical - orthogonal frequency division multiplexing (DCO-OFDM) waveform to achieve a high spectral efficiency.

The concept of index modulation (IM) schemes have recently drawn a lot of interest [6]–[9]. Generally, IM introduces additional dimensions for data modulation. Data can be encoded in the space, time and subcarrier index to improve

energy and spectral efficiency. Numerous IM schemes focus on modulating the indices of subcarriers in subcarrier-index modulation (SIM) [10]–[16]. Using the indexes of LEDs for modulation, spatial modulation (SM) has been widely considered in recent years [17]–[19]. Similarly, numerous other studies on space-time index modulation can be noted [20]–[23]. Unlike the existing IM works, we propose a novel application of IM for LiFi dimming, in which TIM is chosen for several reasons. Firstly, TIM is more suitable for single light emitting diode (LED) transmission since dimming codes are applied in the time domain. This makes TIM compatible with the existing lighting infrastructure because LEDs within a light source are usually connected to each other. Secondly, a TIM encoder operates entirely in the time domain and it can be additionally used at the output of an OFDM encoder; thus no modification of OFDM encoder is needed. This makes iDim versatile to any OFDM encoder/decoder. Moreover, TIM uses a simple encoding/decoding technique in the time domain, which is advantageous to reduce the implementation complexity. iDim is able to benefit from using TIM, so iDim gains benefits in many ways compared to other dimming methods. Notable benefits include a high communication performance, a wide dimming range, and a high transmission rate. The outstanding performance of iDim over existing methods will become more evident through the experimental results. Additionally, we propose two types of dimming codes. These codes provide a high coding rate and a high bit error ratio (BER) performance, which significantly contribute to the overall targets of the iDim system.

Until this date, the number of experimental studies on IM is modest. Similarly, even though there are numerous studies on LiFi dimming techniques [24]–[28], the number of implementation studies, such as [29], [30], is still few. A notable PWM-inspired dimming method for multi-carrier waveforms was proposed in [28]. By inserting inactive slots, it can control the dimming based on the ratio of the inserted inactive slots within the OFDM frame. This could significantly extend the dimming range and remove the problem of non-zero optical power at the 0% brightness level. For comparison purposes, we refer to this scheme [28] as 'sDim'. The drawback of the sDim method is a significantly reduced transmission rate [28]. When comparing to sDim, the proposed iDim scheme has the same dimming capability as sDim. However, iDim gains additional spectral efficiency due to the use of index modulation. More importantly, to the best of our knowledge, the proposed iDim is the first implementation of an efficient index modulation technique designed for LiFi dimming.

The remainder of this paper is organized as follows. Section II introduces the benefits of the proposed iDim scheme by comparing it to related works. Section III explains the system implementation architecture, system model and theoretical analysis, and the methods to evaluate the system. Section IV explains the generation of line codes for TIM and presents their experimental performance. Moving on, Section V demonstrates the experimental results of the iDim system, including the SNR quality, transmission rate, and energy efficiency. Finally, Section VI concludes the work.
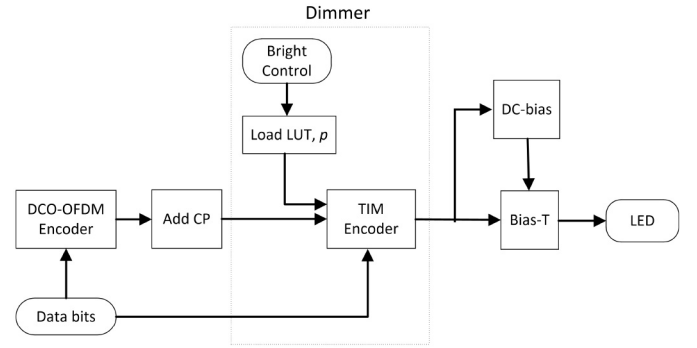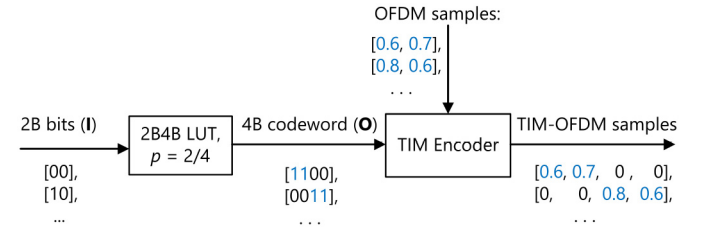

Fig. 1.   iDim- DCO-OFDM transmitter block diagram.

Fig. 2.   Illustration of the TIM encoding process within iDim system when applying 2B4B code with the dimming parameter p of 2/4.

II. SYSTEM ARCHITECTURE AND THEORETICAL ANALYSIS

A. System Operation

1) Transmitter Operation: The block diagram for the transmitter (TX) is illustrated in Fig. 1. Notice that the DCO-OFDM encoder does not require any modification. The brightness controlling block (referred to as a dimmer) is located at the output of DCO-OFDM encoder. The most significant element of the dimmer is a TIM encoder. Based on the selected dimming level, a mBnB code from the lookup table (LUT) is chosen, and the dimming parameter $p \subset \{1/n, 2/n, \ldots, (n-1)/n\}$ (where p is the weight of the binary line code) is set for the TIM encoder. The LUT generation is detailed in **Algorithm 1**. Based on that code, the TIM encoder maps its data bits to decide the indices of the active OFDM samples and inactive samples within the time-domain frame. The inactive samples refer to the samples where the LED is turned off.

Particularly when the line code mBnB and the dimming parameter p are loaded, the TIM encoder selects a mapping column from the LUT for a specific mapping rule (mapping from an input codeword **I** to an output codeword **O**). The encoder takes $k = pn$ OFDM samples as an input and inserts $n - k = (1 - p)n$ inactive samples. Thus, there will be totally n samples at the output of the TIM encoder. The index dimension, which represents the indices of the active OFDM samples, allows us to encode an additional m data bits.

Fig. 2 illustrates an example of iDim encoding when applying a line code 2B4B ($n = 4$) with the dimming parameter $p = 2/4$. The 2B4B LUT allows for mapping from a 2-bits codeword **I** to a 4B codeword **O**. After mapping, based on the 4B codeword, the TIM encoder allocates the positions of OFDM samples and inactive samples.
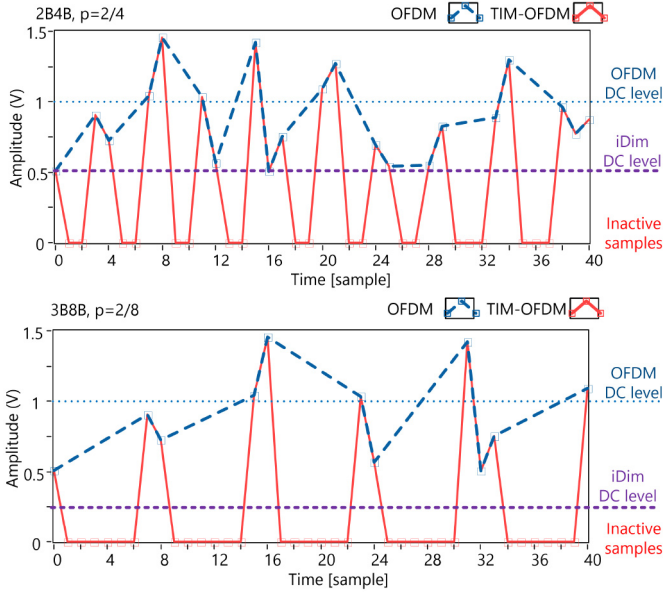
Fig. 3. Examples of iDim waveform: Applying 2B4B code with the dimming parameter p of 2/4 (top), and applying 3B8B code with the dimming parameter p of 2/8 (bottom).

Fig. 3 illustrates two examples of iDim waveform using different line codes. Particularly when a line code 2B4B ($n = 4$) with the dimming parameter $p = 2/4$ are loaded (the top subfigure), the TIM encoder takes $k = pn = 2$ OFDM samples and inserts $n - k = 2$ inactive samples. This encoding period produces 4 TIM-OFDM samples. The positions of 2 inactive samples being inserted depend on the data bits ($m = 2$ bits) being encoded by the TIM encoder. Similarly, when a line code 3B8B ($n = 8$) and the dimming parameter $p = 2/8$ are loaded (the bottom sub-figure), the TIM encoder generates 8 TIM-OFDM samples from $k = pn = 2$ OFDM samples and $n - k = 6$ inactive samples. For both examples, the iDim DC-level is adjustable according to the OFDM activation ratio (which equals to the dimming parameter p) while the OFDM peak-to-peak amplitude is kept constant. This allows controlling the brightness and avoiding the reduction of the OFDM signal amplitude (avoid using AM dimming).

2) Receiver Operation: The block diagram for the receiver (RX) is illustrated in Fig. 4. The TIM decoder is located after the synchronization and cyclic prefix (CP) removal blocks and before the fast Fourier transform (FFT) block, and it operates entirely in the time domain as detailed in **Algorithm 2**. There is no modification to the DCO-OFDM decoder. Finally, data bits coming out from the two decoders are merged.

B. System Model and Performance Metrics

The received signal $\mathbf{y}$ can be expressed by:

$$\mathbf{y} = \mathbf{h}\mathbf{x} + \mathbf{z} \qquad (1)$$

where $\mathbf{h}$ denotes the channel matrix in the time domain, $\mathbf{x}$ denotes the transmitted signal, and $\mathbf{z}$ denotes the AWGN noise.

1) TIM Demodulation: The matched filter (MF) with filter coefficients $\mathbf{b}$ is used in the TIM demodulation process, where $\mathbf{b} = [\mathbf{1}_{1 \times k} \; -\mathbf{1}_{1 \times n-k}]$; $\mathbf{1}_{1 \times k}$ is a set of k binaries 1;
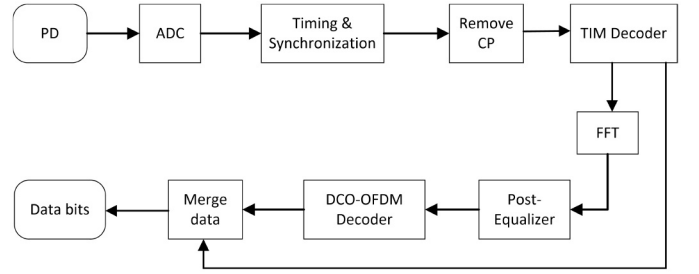

Fig. 4. iDim- DCO-OFDM receiver block diagram.

$-\mathbf{1}_{1 \times n-k}$ is a set of $(n - k)$ binaries -1; and $k = pn \subset \{1, 2, \ldots, n\}$. The output of MF is a cost function which results from the convolution of all cases of shifting the received signal $\mathbf{y}$ to the left hand side by $(j - 1)$ binary digits (where $j \subset \{1, 2, \ldots, n\}$) and the MF $\mathbf{b}$. For each case of j, the cost function is calculated as:

$$C_j = \sum_{u=j}^{j+np} y_u - \sum_{v=j+np+1}^{j+n+1} y_v \qquad (2)$$

where $y_u, y_v \subset \mathbf{y}$ are the signal samples.

From the values of the cost function $\{C_j\}$, the TIM decoder finds the index ϕ that satisfies: $C_\phi = \mathrm{Max}\{C_j\}$. Based on this index ϕ, the decoder lookup the mapping table LUT for the output data bits $\mathbf{I}[\phi]$. The SNR in dB at the output of the MF based TIM decoder is measured as:

$$\beta = 20 \log\left(\frac{u}{\sigma}\right) \qquad (3)$$

where u denotes the minimum Euclidean distance between the MF output symbols; σ denotes the error vector magnitude (EVM) of the matched symbols C_ϕ.

2) OFDM Demodulation: After the TIM demodulation, the OFDM samples are extracted and the OFDM demodulation is executed. When the matched index ϕ is wrong, the extraction of a set of k OFDM samples is incorrect. Overall, this wrong TIM demodulation will dismiss OFDM samples and replace them by inactive samples. Because inactive samples are zero-values, the set of samples being fed into the OFDM decoder (denoted as $\mathbf{y}_\omega$) is expressed as:

$$\mathbf{y}_\omega = \mathbf{h}(\mathbf{x} - \mathbf{x}_\omega) + \mathbf{z} \qquad (4)$$

where $\mathbf{x}_\omega$ denotes the error signal due to the imperfect TIM demodulation. At a time instance i, $\mathbf{x}_\omega[i] = 0$ means there is no error, while $\mathbf{x}_\omega[i] = \mathbf{x}[i]$ means that an OFDM sample $\mathbf{x}[i]$ is replaced by an inactive sample.

By considering the impact of imperfect TIM demodulation, the OFDM demodulation now becomes:

$$\mathbf{Y}_\omega = \mathrm{FFT}\{\mathbf{h}(\mathbf{x} - \mathbf{x}_\omega) + \mathbf{z}\} = \mathrm{FFT}\{\mathbf{h}\,\mathbf{x} + \mathbf{z}\} - \mathrm{FFT}\{\mathbf{h}\mathbf{x}_\omega\} \qquad (5)$$

where $\mathbf{Y}_\omega$ is the signal in the frequency domain that considers the imperfect TIM demodulation; FFT{} is the fast Fourier transform.

We can simply express $\mathbf{Y}_\omega$ with the impact of imperfect TIM demodulation as:

$$\mathbf{Y}_\omega = (\mathbf{Y} + \mathbf{Z}) - \delta\mathbf{Y} = (1 - \delta)\mathbf{Y} + \mathbf{Z} \qquad (6)$$

where δ denotes the energy contribution factor from the dismissed OFDM samples caused by the wrong TIM demodulation; $(1 - \delta)$ is the signal energy reduction factor which is caused by the dismissal of several OFDM samples. The symbols **Y** and **Z** represent the signal and the AWGN noise respectively.

The energy reduction factor $(1 - \delta)$ depends on the ratio of the number of the dismissed OFDM samples (caused by the TIM demodulation error) to the total number of OFDM samples within an OFDM frame. This leads to the energy reduction of all subcarriers. Thus, it will reduce the average SNR performance measured at the output of the OFDM decoder.

The OFDM communications performance is also evaluated by measuring the SNR (denoted as γ) [31] at the output of the OFDM decoder. Similar to the SNR calculation for the TIM decoder, the SNR of the OFDM decoder, in dB, where M-QAM is used with M is the constellation size, is measured as:

$$\gamma = 20 \log \left(\frac{u_{\text{QAM}}}{\sigma_{\text{QAM}}} \right) \tag{7}$$

where u_{QAM} denotes the minimum Euclidean distance of the considered QAM order, and σ_{QAM} denotes the EVM of the received QAM symbols.

C. Transmission Rate Calculation

1) Traditional DCO-OFDM Transmission Rate: Because of the Hermitian symmetry mapping rule for producing a real valued time-domain waveform, the total data bits carried by one DCO-OFDM frame is:

$$D_1 = (N_{\text{FFT}}/2) \log_2 \left(N_{\text{QAM}} \right) \tag{8}$$

where N_{FFT} is the FFT size, and N_{QAM} is the QAM modulation order.

The DCO-OFDM frame has the length of $T_1 = N_{\text{FFT}}$ samples. Thus, the transmission rate of DCO-OFDM is:

$$R_1 = D_1 / T_1 = (1/2) \log_2 \left(N_{\text{QAM}} \right). \tag{9}$$

2) iDim DCO-OFDM Transmission Rate: In the proposed iDim system, when a line code mBnB is loaded, the TIM encoder takes $(p\,n)$ OFDM samples as an input, and it encodes them to produce n samples at the output. The index dimension allows us to encode an additional m data bits. Both the TIM encoder and the OFDM encoder carry data bits. The total transmission rate is calculated step by step as follows.

Firstly, when the TIM encoder uses a line code mBnB, it expands the length of the OFDM frame. The OFDM frame is now longer than the original OFDM frame at the ratio of $n/m = 1/p$. Therefore, the transmission rate of the DCO-OFDM encoder is now reduced as:

$$R_1' = (p/2) \log_2 \left(N_{\text{QAM}} \right) \tag{10}$$

Secondly, the TIM encoder adds m data bits for a set of $(p\,n)$ OFDM samples. This contributes to the total transmission rate. The total number of TIM encoding bits carried by encoding one OFDM frame is:

$$D_2 = m \left[N_{\text{FFT}}/(p\,n) \right] \tag{11}$$

Because the index-encoded OFDM frame now has the length of $T_2 = N_{FFT}/p$ samples, this results in the transmission rate of the TIM encoder:

$$R_2' = D_2 / T_2 = m/n \tag{12}$$

Combining Eqs. (10) and (12), the total transmission rate of the iDim DCO-OFDM system is calculated as:

$$R_2 = R_1' + R_2' = (1/2) \left[p \log_2 \left(N_{\text{QAM}} \right) + 2m/n \right] \tag{13}$$

For convenience, we typically use the $\log_2(N_{\text{QAM}})$ value as the transmission rate of DCO-OFDM. Accordingly, for comparison purposes, the normalized transmission rate of the iDim DCO-OFDM can be re-written as:

$$R = p \log_2 \left(N_{\text{QAM}} \right) + 2(m/n) \tag{14}$$

Eq. (14) shows that the normalized transmission rate varies based on the optical power imposed by the dimming parameter p and the coding rate m/n of the line code.

3) sDim DCO-OFDM Transmission Rate: It is unfair to compare the transmission rates of the original DCO-OFDM and the proposed iDim DCO-OFDM because the original DCO-OFDM cannot support such a wide dimming range as that of iDim. Therefore, the sDim scheme is used for comparison. Note that sDim is also a special case of iDim that does not modulate any information on the index of the active OFDM samples. The transmission rate of sDim is:

$$R = p \log_2 \left(N_{\text{QAM}} \right). \tag{15}$$

D. Experimental Setup

The hardware configuration for the iDim DCO-OFDM implementation is illustrated in Fig. 5. It is based on a National Instruments (NI) real-time processing platform, PXIe-1085 computer, which is equipped with field programmable gate array (FPGA) NI-7966R panels. An analog-to-digital/ digital-to-analog (ADC/DAC) board (NI-5781, 20 MHz communication bandwidth) operates in the baseband to allow for intensity modulation with direct detection. An alternating current (AC)-coupled Photodiode (PD) (Femto-HSPR-X-I-1G4-SI with a 3-dB bandwidth of 1.4 GHz), and an off-the-shelf LED (Vishay VLMB1500) are used to detect and transmit the signal, respectively. An additional programmable DC generator (Keysight E36313A) is connected to the DC input of the bias-T to supply the LED with a controllable bias voltage.

A wide dimming range is one of the goals for the iDim system. To compare the dimming range between the considered schemes, the optical power is measured at the receiver position using the optical power meter PM100USB and the S121C photodiode power sensor at a distance of 0.5 m.

III. GENERATION AND PERFORMANCE OF LINE CODES

A. Generation of Type I Line Codes

Two novel sets of line codes are proposed to enable dimming in TIM. The first set of line codes include the codes 2B4B, 3B8B, and 4B16B, and so on. These codes are called type I line codes. They are simply generated as given in **Algorithm 1**.
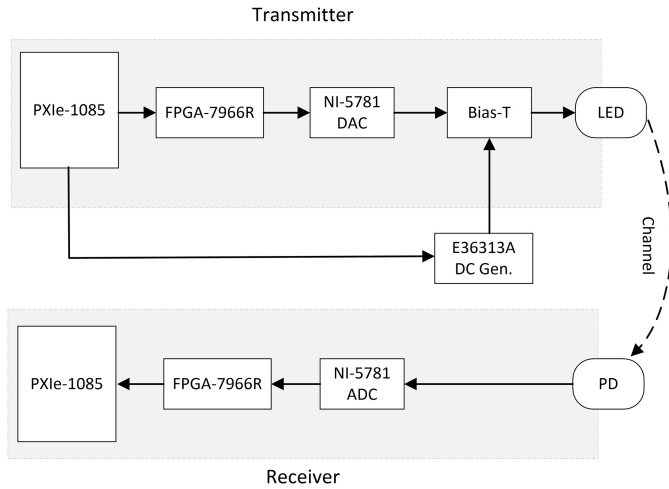
Fig. 5. iDim- DCO-OFDM system implementation architecture.

Algorithm 1: GENERATION OF mBnB LUT

Initialize: m bits input codeword $= \mathbf{I}$; n bits output codeword $= \mathbf{O}$
For: $k \subset \{1, 2, \ldots, n-1\}$
  Calculate: dimming parameter $p = k/n$
  Generate O[1]: the first output codeword as:
$\mathbf{O}[1] = [\mathbf{1}_{1\times k} \ \mathbf{0}_{1\times n-k}]$
  For: $i \subset \{1, 2, \ldots, n\}$
    Generate O[i]: the output codeword with index i $\mathbf{O}[i]$ is generated by shifting the $\mathbf{O}[1]$ codeword to the right hand side (RHS) $(i-1)$ binary digits
  End for
End for
Map data bits: Map the data bits for input codewords $\mathbf{I}[i]$, where $i \subset \{1, 2, \ldots, n\}$
Finish the LUT mapping for different p.

To easily understand the LUT mapping rule, Table I presents an example of the 2B4B code. In the mapping, the binary '1' represents a time slot for an OFDM sample while '0' represents a time slot for an inactive sample where the LED is turned off.

A matched filter (MF) is proposed to maximize the decoder performance. The MF decoding rule is given in **Algorithm 2**. The design of the MF allows us to integrate all codes within the same system.

B. Generation of Line Codes Type II

The second type of line codes (type II) aims to maximize the coding rate for TIM encoding. Unlike the 1:1 mapping rule of the type I line codes, we additionally apply the concept of running disparity (RD) for generating the type II codes. RD allows us to design a better coding rate than that of the type I codes; however, it requires a higher mapping complexity.

The availability of the type II line codes is explained in Appendix B. Accordingly, the type II line codes include the codes 2B3B, 3B4B, and 4B5B.

Because of the mapping complexity, we only describe the 2B3B code as an example. The mapping rule for other codes

---

Algorithm 2: MATCHED FILTERED mBnB DECODING

Initialize: Collect the received waveform set size n as:
$\mathbf{R}[1] = \{y_1, y_2, \ldots, y_n\}$
Define: a matched filter (MF) $\mathbf{b} = [\mathbf{1}_{1\times k} \ -\mathbf{1}_{1\times n-k}]$,
where $k = pn$
For: each index $j \subset \{1, 2, \ldots, n\}$
  Generate R[j]: shifting the $\mathbf{R}[1]$ to the left hand side (LHS) $(j-1)$ binary digits.
  Matched filtering R[j] with filter coefficients $\mathbf{b}$ to have the MF cost function C_j as given in Eq. (2)
End for
Process: Find the index ϕ that satisfies:
$C_\phi = \text{Max}\{C_j\}, j \subset \{1, 2, \ldots, n\}$
Lookup bits: Lookup the LUT at the matched index ϕ for the data bits codeword: $\mathbf{I}[\phi]$.

TABLE I
EXAMPLE OF 2B4B LOOKUP TABLE (LUT)

2B Input (**I**)	4B Output (**O** with p=1/4)	4B Output (**O** with p=2/4)	4B Output (**O** with p=3/4)
00	1000	1100	1110
01	0100	0110	0111
10	0010	0011	1011
11	0001	1001	1101

such as 3B4B and 4B5B is also simple to follow. We apply the 1:1 mapping rule if possible (the same as the type I codes), and then the RD concept will take care of the remaining cases by pair-mapping.

There are two versions of 2B3B codes as given in Tables II and III. Table II generates long-term DC-balanced outputs, while Table III generates short-term DC-balanced outputs. Notice that the Hamming distance (HD) of 2B3B mapping outputs is 1, for all levels of p, which is a half of that of the type I codes. The average Hamming distance is 7/4. This explains a trade-off between the code rate and the transmission performance.

In table II, we note that the long-term DC balanced code may potentially cause flickering. For example, flickering may happen in cases where the interval between the pair of "11" input symbols is long enough to generate a perceptible brightness change. Fortunately, this flickering issue is avoidable by using a simple treatment to generate a constant DC-level for every short time period. Particularly, after mapping, we periodically insert 3B bit redundancy so that the period of samples is always DC-balanced.

A short-term DC balanced mapping for 2B3B in Table III uses a technique called paired mapping. Whenever the symbol "11" appears, the encoder takes "11" and the following two bits for mapping at the same time. This method is flicker-free because of the short-term DC balance property of any adjacent 6B outputs.

Finally, we note that there is no common matched filter decoding rule for the type II codes as there is for type I codes.

TABLE II
2B3B LUT (LONG-TERM DC VERSION)

	2B Input (**I**)	3B Output (**O** with p=1/3)	3B Output (**O** with p=2/3)
I$_1$	00	100	110
I$_2$	01	010	011
I$_3$	10	001	101
I$_4$	11	000 - 110	100 - 111

The running disparity ± 1 is applied for the outputs of **I**$_4$.

TABLE III
2B3B LUT (SHORT-TERM DC VERSION)

	2B Input (**I**)	3B Output (**O** with p=1/3)	3B Output (**O** with p=2/3)
I$_1$	00	100	110
I$_2$	01	010	011
I$_3$	10	001	101
I$_4$ -**I**$_x$	11- 00	000 - 110	100 - 111
	11 - 01	011 - 000	111- 010
	11 - 10	000 - 101	001 - 111
	11 - 11	101 - 000	111 - 001

where **I**$_x \subset \{$**I**$_1,$**I**$_2,$**I**$_3,$**I**$_4\}$ is the next 2B input being encoded at the same time with **I**$_4$. The running disparity ± 1 is applied for the pair-mapping in the cases of **I**$_4$.

The decoder of the type II codes will directly use the LUT mapping binary outputs as the filter coefficients to search for the optimal match.

C. Simulation Performance - Type I Codes

The simulations evaluate the BER performance of proposed line codes under different channel conditions (the channel SNR is in dB). For performance comparison purposes, a standard code On Off Keying (OOK) is used. The MF design given in **Algorithm 2** significantly improves the BER performance of the proposed line codes. The simulation results are shown in Figs. 6 and 7 for 2B4B and 3B8B, respectively. The results show that the proposed codes require 3 dB to 5 dB less SNR than OOK to achieve the same BER, demonstrating the benefit of the MF.

Additionally, the performance of different line codes is examined under different dimming conditions by comparing the performance of the same code and applying a different value for the dimming parameter p. The code 2B4B achieves almost the same BER performance for all the considered dimming levels. Codes 3B8B and 4B16B have 1 dB difference between the lowest/highest brightness levels and the remaining brightness levels. Particularly within 3B8B, the BER performance at $p = 1/8$ is exactly the same as that at $p = 7/8$; and both require 1 dB more SNR than the remaining values of p (i.e., $p = 2/8$ to $p = 6/8$) to reach the same
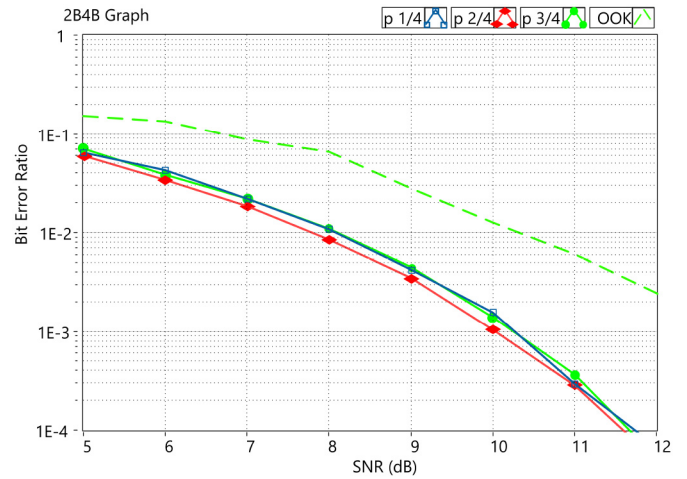

Fig. 6. Simulated BER performance of matched filtered 2B4B versus OOK.
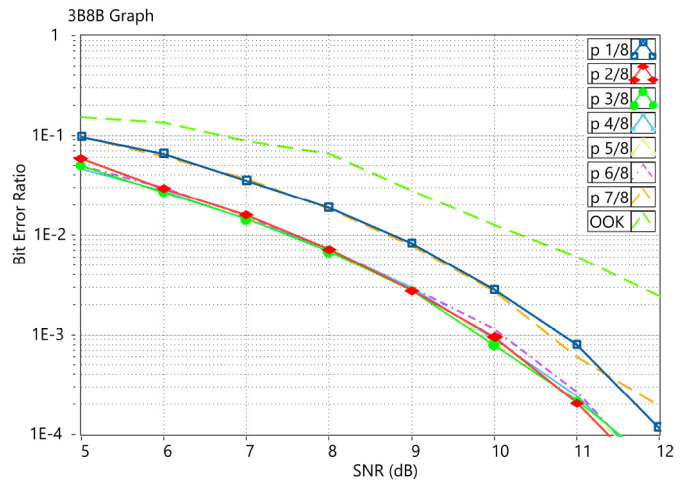

Fig. 7. Simulated BER performance of matched filtered 3B8B versus OOK.

BER. This is due to the unequal average Hamming distance between the line codes at different values for p. Overall, the lowest performance case of 3B8B (with MF) still outperforms that of OOK.

D. Simulation Performance - Type II Codes

The type II line codes have a trade-off between the code rate and the performance. While they offer higher code rates than that of the type I line codes, their BER performance is lower. This is because of their lower HD between the output codewords; for example, the 2B3B codes have an HD of 1, which is half that of the type I line codes.

The 2B3B has a complex mapping rule, thus it directly uses the LUT for matching and decoding. Fig. 8 presents the BER performance of 2B3B short-term DC and long-term DC versions. The results do not show different BER curves for different values of p ($p = 1/3$ or 2/3), because 2B3B codes have an equal average HD for different p.

Similar to the type I line codes, the results also show that the MF significantly improves the BER performance. Specifically, by targeting the same BER, the MF codes gain about 3 dB to 5 dB less SNR comparing to the original codes without MF.
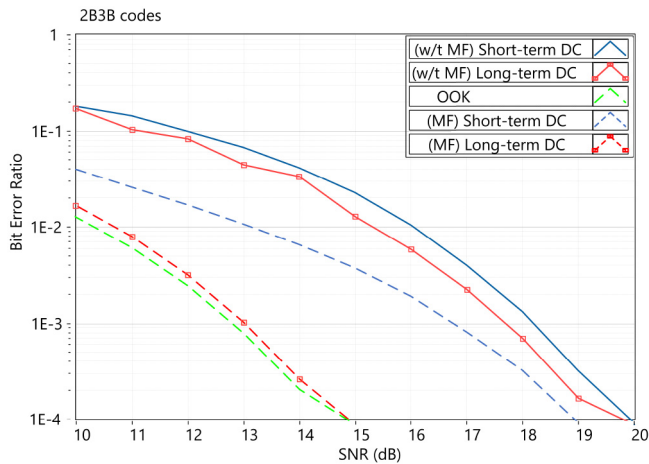
Fig. 8. Simulated BER performance of different 2B3B codes (with/without MF) versus OOK.
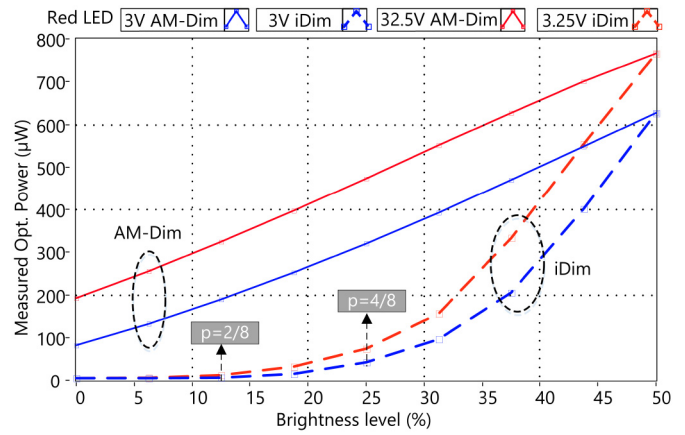

Fig. 9. Measurement of optical power at the distance of 0.5 m from the LED when applying AM-dimming and iDim to DCO-OFDM. Note that iDim provides a consistently high SNR of 22.5 dB while AM-dim reduces SNR significantly at low brightness levels.
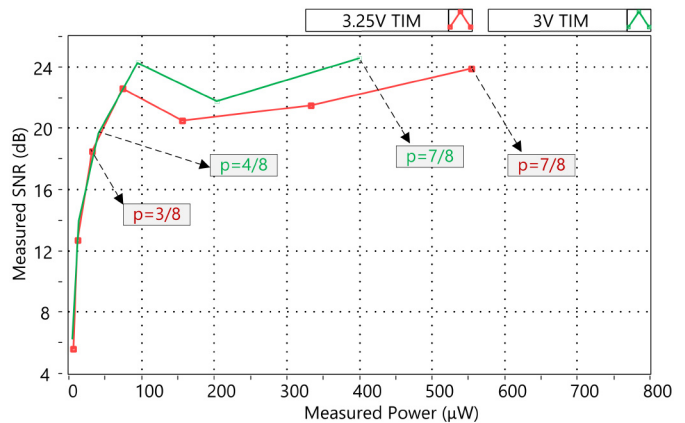

Fig. 10. Measured performance of TIM decoder in iDim DCO-OFDM system (3 V and 3.25 V bias voltages).

When comparing the two versions of 2B3B, the long-term DC version achieves a higher BER than the other. This is because the mapping rule in the long-term DC version is less complex, thus the error caused by a hard-thresholding decision between the cases is less. However, the best BER case of both 2B3B versions (the long-term DC code with MF) is close to the BER of OOK because both OOK and 2B3B have the HD of 1.

E. Optical Link Implementation

Two goals were achieved in the implementation of a TIM encoder within the iDim DCO-OFDM system. Firstly, the measured optical power reaches an extremely low value (20 μW) during the data communication at the bandwidth of 20 MHz. Secondly, the SNR performance of both TIM and DCO-OFDM decoders is high for all dimming levels (above 17 dB). This ensures a reliable communication performance for the TIM encoder within the proposed iDim system when dimming is applied.

Fig. 9 presents the measured optical power for AM-dimming and iDim. The minimum achievable optical power (without any data communications) of the AM-dimming scheme is about 200 μW and 90 μW in the cases of 3.25 V and 3 V bias voltages, respectively, for a given LED. On the other hand, iDim achieves an optical power that is about 20 μW at $p = 1/8$ for all bias voltages. This is a 10 times and 4.5 times optical power reduction, respectively.

The measurement of the SNR in the optical links is shown in Fig. 10. Bias voltages of 3 V and 3.25 V are both considered. The TIM decoder shows a consistently high performance for both bias voltage cases. More particularly, an SNR above 20 dB can be achieved for all optical power levels above 40 μW (equivalent to p levels above 4/8). Overall, the TIM achieves a high SNR performance at an extremely low optical power of 40 μW.

IV. PERFORMANCE OF iDIM DCO-OFDM

A. Optical Link Quality

This section compares the performance of the DCO-OFDM decoder in the AM-dimming system to the implementation of DCO-OFDM in the iDim system. The system setup specifications are summarized in Table IV. It is noted that the operating communication bandwidth of 20 MHz is considered as a flat channel and the inter-sample interference can be ignored in the SNR measurement. However, when the channel is not flat and the inter-sample interference is high, pulse shaping techniques (with Raised-Cosine (RC), Root Raised Cosine (RRC), and Gaussian filters) can be additionally used. Due to the limited space, details of the pulse shaping techniques are not included in this paper.

Fig. 11 shows the SNR measurement results. Both bias voltages of 3 V and 3.25 V are considered. The 4-QAM modulation order is chosen for DCO-OFDM for comparison purposes. It is also possible to use other constellation sizes.

At 3 V bias voltage, the performance of the iDim DCO-OFDM system is constant at 23 dB for all dimming levels above $p = 4/8$. As p goes lower, the measured optical power

TABLE IV
SYSTEM SETUP SPECIFICATIONS

|	Specifications
Real-time system	PXIe-1085 computer NI-7966R FPGA NI-5781 ADC/DAC (3 dB bandwidth of 40 MHz) Keysight E36313A DC generator
Front-end devices	Vishay VLMB1500 LED Femto-HSPR-X-I-1G4-SI PD (3 dB bandwidth of 1.4 GHz)
Optical power measurement	Optical power meter PM100USB Photodiode power sensor S121C
OFDM parameters	FFT size of 64 CP size of 16 4 QAM modulation order Operating communication bandwidth of 20 MHz
TIM parameters	Type I codes: 2B4B/ 3B8B/ 4B16B Type II codes: 2B3B/ 3B4B/ 4B5B Dimming parameter p varies
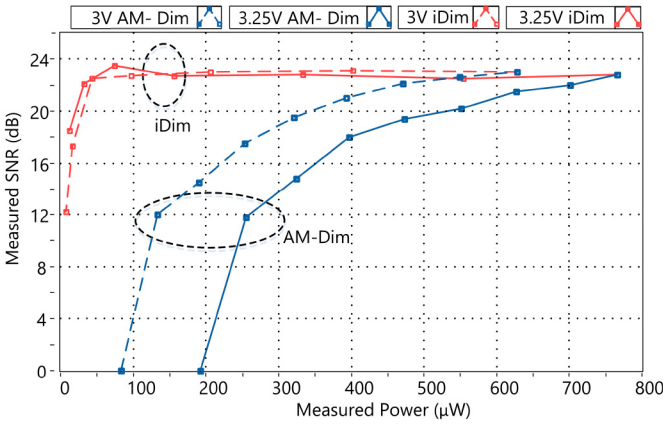
Fig. 11. Measured performance of iDim DCO-OFDM versus AM-dimming DCO-OFDM (3 V and 3.25 V bias voltage).
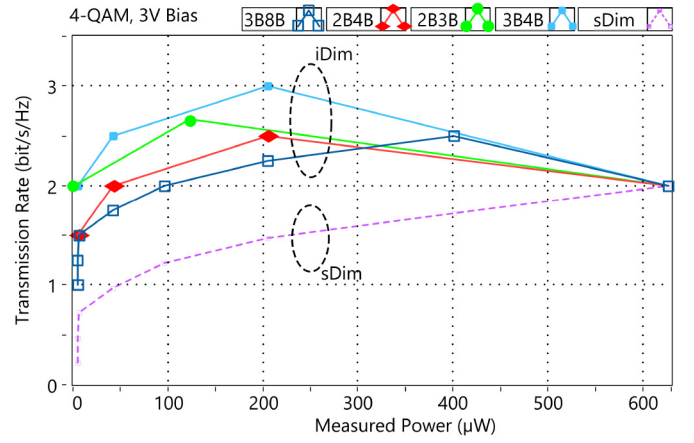

Fig. 12. Achieved Transmission Rate of iDim and sDim versus optical power measured at 0.5 m distance (4-QAM DCO-OFDM, 3V bias).

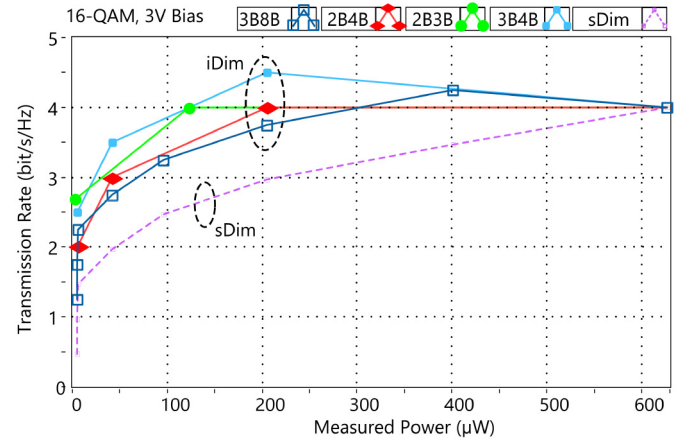Fig. 13. Achieved transmission rate of iDim and sDim versus optical power measured at 0.5 m distance (16-QAM DCO-OFDM, 3V bias).

drops below 40 µW and the corresponding performance starts to degrade (see Fig. 11). The lowest optical power that can guarantee a proper decoding of bits (defined as SNR above 17 dB) is measured at 20 µW. This is significantly lower than the lowest optical power required for the DCO-OFDM decoder of the AM-Dim system that is given at 200 µW. Together with the performance measurement of the TIM decoder, we can conclude that the proposed iDim technique has achieved a consistently high performance during dimming, and reached an extremely low optical power. Moreover, it is important to note that the iDim technique provides a high data rate, resulting in increased energy efficiency.

At 3.25 V bias voltage, the superior performance of iDim is more pronounced. The AM-dimming dissipates at least 350 µW optical power at SNR values above 15 dB. In comparison, the proposed iDim decoders guarantee a high SNR performance of 18 dB at an optical power measured at 20 µW (17.5 times lower).

B. Transmission Rate

The transmission rate gain of our iDim compared to sDim is more pronounced when the measured optical power is considered. Note that sDim is a specific case of iDim without index modulation bits. This comparison is useful to contrast the contribution of index modulation to the total transmission rate when dimming is required.

In cases with 4-QAM (Fig. 12) at any brightness level between 20 µW and 200 µW, the best-rate codes (2B3B and 3B4B) can provide more than double the transmission rate than sDim. Also within the same brightness range, our lowest-rate code 3B8B can provide at least 30% increase in the data transmission rate of sDim. Moreover, for all brightness levels between 20 µW and 640 µW, we always can find a code that provides a higher transmission rate than the maximum rate of 2 bits/Hz of the traditional 4-QAM DCO-OFDM. This means that we jointly gain a wide dimming range, a high SNR, and a transmission rate higher than the maximum of the traditional 4-QAM DCO-OFDM. Note that traditional DCO-OFDM uses AM-dimming and reduces the SNR when the light is dimmed.

Similarly in the case of 16-QAM (Fig. 13) at any brightness level between 20 µW and 400 µW, the iDim scheme also gains
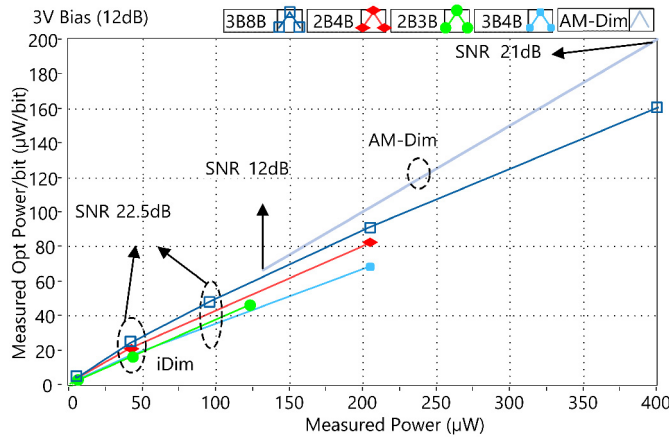
Fig. 14. Measured optical power/bit comparison between AM-Dim and iDim systems (3 V bias voltage).
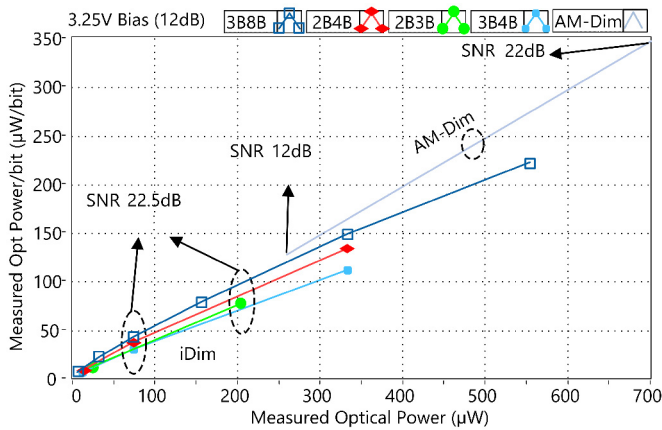

Fig. 15. Measured optical power/bit comparison between AM-Dim and iDim systems applied for 4-QAM DCO-OFDM (at 3.25V bias, 12dB SNR limit).

transmission rates, which are from 18% to 40% higher than the sDim, depending on the codes and the brightness level. On the other hand, for all cases with an optical power above 120 μW, there exists a code to achieve an equal or a better code rate than 4 bits/Hz (this is the maximum transmission rate of the original DCO-OFDM when dimming is not supported).

C. Energy Efficiency

The measured results of optical power/bit are shown in Figs. 14 and 15. The proposed iDim shows a lower optical power/bit than the AM dimming scheme for all brightness levels. Moreover, it showcases the ability of iDim to reach extremely low optical power values.

Particularly in Fig. 14 (3 V bias voltage), at 130 μW, AM-dimmed DCO-OFDM requires 66 μW/bit while 2B4B iDim and 2B3B iDim use 55 μW/bit and 45 μW/bit, saving 17% and 30% of the energy respectively. For any brightness below 130 μW, AM-dimmed DCO-OFDM cannot guarantee at least 12 dB SNR, while iDim maintains a 22.5 dB SNR and linearly reduces the required optical power/bit. This results in a dual gain in the achieved SNR and optical power/bit requirement.

Similarly in Fig. 15 (3.25V bias voltage), the lowest optical power that AM-dimmed DCO-OFDM can maintain the 12 dB

SNR level is 255 μW. In comparison, iDim maintains the peak SNR of 22.5 dB for all considered brightness levels. At this 255 μW optical power level, the AM-dimming still requires 127 μW/bit while 2B4B and 3B4B iDim schemes use 78% and 70% of that optical power/bit, respectively. For a better understanding of the benefits of the gain of optical power/bit from the proposed iDim system, the calculations of optical power/bit for the system using different line codes are given in Appendix A.

V. CONCLUSION

A novel dimming method is proposed in this paper, termed indexed dimming method (iDim). The integration of the TIM and DCO-OFDM is demonstrated in this proof-of-concept study. Two types of line codes aimed at dimming are proposed for TIM. The proposed solution results in a reliable link quality, as proven by simulations and experimental results.

The measurement results of the optical power and the SNR for the proposed system show the advantages of the iDim system. The proposed solution guarantees a high communication performance during dimming, which is measured in a minimum SNR of 20 dB. In comparison, existing methods such as AM diming reduces the communication performance significantly to below 10 dB. The proposed iDim achieves a wide dimming range that extends beyond existing dimming solutions such as AM dimming. The proposed system can maintain a reliable communication link at extremely low optical power of 20 μW, which is ten times lower than the limits of all existing solutions. Moreover, the proposed solution improves the spectral efficiency of all the existing dimming techniques using TIM.

APPENDIX A
CALCULATION OF DIMMING RANGE AND OPTICAL POWER/BIT

We calculate the optical power/bit for different dimming schemes. Table V summarizes the calculation of the normalized transmission rate and the optical power consumption of DCO-OFDM (without dimming), AM-Dim DCO-OFDM, sDim DCO-OFDM, and iDim DCO-OFDM. It is noted that, AM-dimming provides the lowest optical power of $\{P_0 + \alpha P_{50}\} \to P_0$ that happens when the amplitude scaling factor $\alpha \to 0$ (thus, $P_0 > 0$ is the offset optical power measured at the 0% AM-dimming level). When comparing to AM dimming, iDim offers the lowest optical power of $\lambda p P_0 \to 0$ that happens when $p \to 0$. This explains why there is a zero offset optical power in the proposed iDim.

We now compare the optical power/bit of iDim and sDim at different dimming levels to show the benefit of index modulation bits to the total transmission rate. Let P_s be the optical power/bit of the sDim DCO-OFDM, and P_i be the optical power/bit of the iDim DCO-OFDM. When a line code mBnB and a dimming parameter p are used, the gain in optical power/bit by using index modulation is calculated as:

$$\frac{P_s - P_i}{P_s} = \frac{2m/n}{p\{\log_2 N_{\text{QAM}}\} + 2m/n} \tag{16}$$

TABLE V
COMPARISON OF TRANSMISSION RATE AND OPTICAL POWER BETWEEN
DIFFERENT DIMMING SCHEMES

Scheme	Transmission Rate	Optical Power
(without dim) DCO-OFDM	$\log_2 N_{QAM}$	$P_0 + P_{50}$
AM-Dim DCO-OFDM	$\log_2 N_{QAM}$	$P_0 + \alpha P_{50}$
sDim DCO-OFDM	$p(\log_2 N_{QAM})$	$\lambda p(P_0 + P_{50})$
iDim DCO-OFDM	$p(\log_2 N_{QAM}) + 2(m/n)$	$\lambda p(P_0 + P_{50})$

where $\alpha < 1$ denotes the amplitude scaling factor of AM-dimming; $\lambda < 1$ is the correction factor that relates to the nonlinear electrical-to-optical conversion when p changes; P_0 is the offset optical power of the AM dimming that is measured at the 0% dimming level; P_{50} is the optical power that DCO-OFDM uses at the 50% dimming level; m/n is the coding rate of the mBnB line code used in the iDim system.

TABLE VI
GAIN OF OPTICAL POWER/ BIT BY USING INDEX MODULATION WITH
DIFFERENT CODES AND p

Scheme	Optical power/bit Gain (4-QAM)	Optical Power/bit Gain (16-QAM)
sDim	0	0
3B8B iDim	$(6/8)/(2p+6/8)$	$(6/8)/(4p+6/8)$
2B4B iDim	$1/(2p+1)$	$1/(4p+1)$
2B3B iDim	$(4/3)/(2p+4/3)$	$(4/3)/(4p+4/3)$
3B4B iDim	$(6/4)/(2p+6/4)$	$(6/4)/(4p+6/4)$

TABLE VII
NUMERIC RANGE OF THE OPTICAL POWER/BIT GAIN BY INDEX
MODULATION

Scheme	Optical power/bit Gain (4-QAM)	Optical power/bit Gain (16-QAM)
sDim	0	0
3B8B iDim	0.3 - 0.75	0.18 - 0.6
2B4B iDim	0.4 - 0.67	0.25 - 0.5
2B3B iDim	0.5 - 0.67	0.33 - 0.5
3B4B iDim	0.5 - 0.75	0.33 - 0.6

Particularly when 4-QAM and 16-QAM modulation orders are used, the gain of optical power/bit at a dimming parameter p is calculated in Table VI. For a specific different line code with its known range of p, the range of optical power/bit gain is numerically given in Table VII.

Calculated results in Table VII show that, iDim saves from 30% to 75% of optical power/bit in the case of 4-QAM. Similarly, it saves from 18% to 60% of optical power/bit in the 16-QAM case. This optical power/bit gain varies according to the selection of the line code mBnB and the parameter p.

APPENDIX B
AVAILABILITY OF OTHER LINE CODES

This section examines the availability of other type II line codes based on the combination statistics. To maximize the coding rate, we target the code form $(n-1)$BnB. The availability of a $(n-1)$BnB code depends on the dimming range we target, which is corresponding to the range of $p \subset [1/n, (n-1)/n]$.

Particularly, we consider two cases of the dimming range to design the code as follows.

Case 1: Considering $p = 1/n$ to $p = (n-1)/n$

The input codeword at the length of $(n-1)$ requires $2^{(n-1)}$ different states at the output for mapping. This requirement applies for all different values of the parameter p; however the dimming parameters $p = 1/n$ and $p = (n-1)/n$ are most challenging due to the limited number of the combinations of outputs. If the code at the dimming parameter $p = 1/n$ exits, the code at all other dimming parameters $p \neq 1/n$ will exist. Because the condition for two dimming parameters $p = 1/n$ and $p = (n-1)/n$ are similar, so the case $p = 1/n$ will be explained in this instance.

When $p = 1/n$, there are $C(n, 1) = n$ different ways to allocate a single "1" among others $(n-1)$ "0"s to produce an output codeword. An increase of n will restrict the availability of the code as the value of $2^{(n-1)}$ (the required number of codewords) is getting much larger than n (the available number of codewords). The running disparity (RD) concept is used for the mapping rule as follows.

First, all of the possible codewords with RD = 0 are used for one-input to one-output mapping. This includes all allocations of a single "1" among all-other "0"s must be used. There are $C(n, 1)$ cases with the 'RD = 0' mapping.

Next, a pair of two inputs will be mapped at the same time. The pair of running disparity values RD = ± 1 are alternatively used for the pair of output codewords. This ensures a long-term DC balance for pairs of the output codewords. Because we have used $C(n, 1)$ output codewords for the 'RD = 0' mapping, the remaining number of un-mapped input cases of the 'RD = 0' is:

$$2^{(n-1)} - C(n,1) = 2^{(n-1)} - n. \tag{17}$$

Required number of outputs for RD = ± 1 mapping: We target combining two output codewords at RD = ± 1 (i.e., combining $p = 0/n$ and $p = 2/n$) to reach the average power of $p = 1/n$ in the long-term. Based on the number of un-mapped cases in (17), the required number of output codewords for mapping the RD = ± 1 combination is:

$$\left\{2^{(n-1)} - n\right\} \times \left\{2^{(n-1)} - n\right\}. \tag{18}$$

Available number of outputs for RD = ± 1 mapping: For RD = + 1, there are only $C(n, 2)$ different ways of two "1"s being allocated among other "0"s. For RD = − 1, it is an 'all-zero' pattern. we can insert the 'all-zero' pattern to the left or the right of a RD = + 1 output codeword. Accordingly, we have the maximum number of output codewords as:

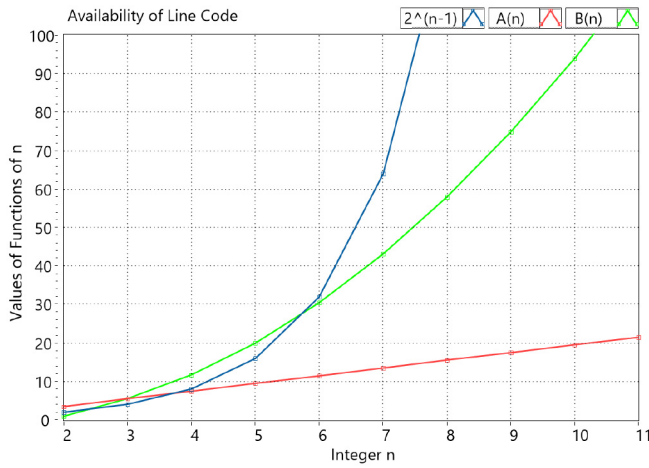$$2C(n,2) = 2n!/\{2!(n-2)!\} = n(n-1) \tag{19}$$

Fig. 16. Test the availability of $(n-1)$BnB line codes using conditions in Eqs. (21) and (23).

Finally, by comparing (18) and (19), the availability of the line code at $p = 1/n$ becomes the availability of an integer n for the following inequality:

$$\left\{2^{(n-1)} - n\right\} \times \left\{2^{(n-1)} - n\right\} \leq n(n-1) \qquad (20)$$

Or it can be re-written as:

$$2^{(n-1)} \leq n + \sqrt{(n(n-1))} = A(n). \qquad (21)$$

Case 2: Considering $p = 2/n$ to $p = (n-2)/n$

The first codes case has clarified the availability of possible codes within the requirement of p ranging from $p = 1/n$ to $p = (n-1)/n$. However, there is one more thing that can be tried by relaxing the requirement of dimming levels. By removing the requirement of the mapping at $p = 1/n$ and $p = (n-1)/n$, the design for outputs at remaining dimming levels $p = 2/n$ to $p = (n-2)/n$ becomes easier. The inequality (20) now becomes less restricted with the following condition:

$$\left\{2^{(n-1)} - C(n,2)\right\}^2 \leq 2\,C(n,1)\,C(n,3) \qquad (22)$$

Or it can be re-written as:

$$2^{(n-1)} \leq \frac{n(n-1)}{2} + \sqrt{\frac{n^2(n-1)(n-2)}{3}} = B(n) \qquad (23)$$

Fig. 16 numerically presents the test of two inequality conditions for Eqs. (21) and (23) which correspond to two cases for the code availability.

For any integer $n > 1$, the inequality (21) is satisfied if and only if $2 \leq n \leq 3$. Therefore, 2B3B provides the best coding rate for the $(n-1)$BnB codes case 1. The LUT for 2B3B has been presented in the body of this paper.

On the other hand, Eq. (23) can be satisfied if $3 \leq n \leq 5$. Thus, it suggests the availability of codes 3B4B and 4B5B. However, a narrower dimming range than the first codes case makes the second codes case less attractive in practice.

REFERENCES

[1] T. Cogalan and H. Haas, "Why would 5G need optical wireless communications?" in *Proc. IEEE 28th Annu. Int. Symp. Pers. Indoor Mobile Radio Commun. (PIMRC)*, Montreal, QC, Canada, 2017, pp. 1–6.

[2] J. Lorincz, A. Capone, and J. Wu, "Greener, energy-efficient and sustainable networks: State-of-the-art and new trends," *Sensors*, vol. 19, no. 22, p. 4864, 2019. [Online]. Available: https://www.mdpi.com/1424-8220/19/22/4864

[3] S. Rajagopal, R. D. Roberts, and S.-K. Lim, "IEEE 802.15.7 visible light communication: Modulation schemes and dimming support," *IEEE Commun. Mag.*, vol. 50, no. 3, pp. 72–82, Mar. 2012.

[4] "Light communication task group (TGbb) documents," IEEE, Piscataway, NJ, USA, Rep. IEEE 802.11, 2021. [Online]. Available: https://mentor.ieee.org/802.11/documents?&is_group=00bb

[5] T. Nguyen, M. S. Islim, and H. Hass, "Integration of dimming into LiFi systems," in *Proc. IEEE 91st Veh. Technol. Conf. (VTC-Spring)*, Antwerp, Belgium, 2020, pp. 1–5.

[6] E. Basar, U. Aygolu, E. Panayırcı, and H. V. Poor, "Orthogonal frequency division multiplexing with index modulation," *IEEE Trans. Signal Process.*, vol. 61, no. 22, pp. 5536–5549, Nov. 2013.

[7] X. Cheng, M. Zhang, M. Wen, and L. Yang, "Index modulation for 5G: Striving to do more with less," *IEEE Wireless Commun.*, vol. 25, no. 2, pp. 126–132, Apr. 2018.

[8] E. Basar, "On multiple-input multiple-output OFDM with index modulation for next generation wireless networks," *IEEE Trans. Signal Process.*, vol. 64, no. 15, pp. 3868–3878, Aug. 2016.

[9] M. Wen, X. Cheng, M. Ma, B. Jiao, and H. V. Poor, "On the achievable rate of OFDM with index modulation," *IEEE Trans. Signal Process.*, vol. 64, no. 8, pp. 1919–1932, Apr. 2016.

[10] F. Halabi, L. Chen, R. P. Giddings, A. Hamié, and J. M. Tang, "Multilevel subcarrier index-power modulated optical OFDM with adaptive bit loading for IMDD PON systems," *IEEE Photon. J.*, vol. 8, no. 6, pp. 1–14, Dec. 2016.

[11] F. Halabi *et al.*, "Subcarrier index-power modulated optical OFDM and its performance in IMDD PON systems," *J. Lightw. Technol.*, vol. 34, no. 9, pp. 2228–2234, May 1, 2016.

[12] N. Ishikawa, S. Sugiura, and L. Hanzo, "Subcarrier-index modulation aided OFDM—Will it work?" *IEEE Access*, vol. 4, pp. 2580–2593, 2016.

[13] R. Abu-Alhiga and H. Haas, "Subcarrier-index modulation OFDM," in *Proc. IEEE 20th Int. Symp. Pers. Indoor Mobile Radio Commun.*, Tokyo, Japan, Sep. 2009, pp. 177–181.

[14] T. Mao, Z. Wang, Q. Wang, S. Chen, and L. Hanzo, "Dual-mode index modulation aided OFDM," *IEEE Access*, vol. 5, pp. 50–60, 2017.

[15] E. Başar, "OFDM with index modulation using coordinate interleaving," *IEEE Wireless Commun. Lett.*, vol. 4, no. 4, pp. 381–384, Aug. 2015.

[16] B. Zheng, M. Wen, E. Basar, and F. Chen, "Multiple-input multiple-output OFDM with index modulation: Low-complexity detector design," *IEEE Trans. Signal Process.*, vol. 65, no. 11, pp. 2758–2772, Jun. 2017.

[17] R. Y. Mesleh, H. Haas, S. Sinanovic, C. W. Ahn, and S. Yun, "Spatial modulation," *IEEE Trans. Veh. Technol.*, vol. 57, no. 4, pp. 2228–2241, Jul. 2008.

[18] M. D. Renzo, H. Haas, and P. M. Grant, "Spatial modulation for multiple-antenna wireless systems: A survey," *IEEE Commun. Mag.*, vol. 49, no. 12, pp. 182–191, Dec. 2011.

[19] P. Yang, M. Di Renzo, Y. Xiao, S. Li, and L. Hanzo, "Design guidelines for spatial modulation," *IEEE Commun. Surveys Tuts.*, vol. 17, no. 1, pp. 6–26, 1st Quart., 2015.

[20] B. Shamasundar, S. Bhat, S. Jacob, and A. Chockalingam, "Multidimensional index modulation in wireless communications," *IEEE Access*, vol. 6, pp. 589–604, 2018.

[21] E. Basar and I. Altunbas, "Space-time channel modulation," *IEEE Trans. Veh. Technol.*, vol. 66, no. 8, pp. 7609–7614, Aug. 2017.

[22] J. Li, M. Wen, X. Jiang, and W. Duan, "Space-time multiple-mode orthogonal frequency division multiplexing with index modulation," *IEEE Access*, vol. 5, pp. 23212–23222, 2017.

[23] S. Jacob, T. L. Narasimhan, and A. Chockalingam, "Space-time index modulation," in *Proc. IEEE Wireless Commun. Netw. Conf. (WCNC)*, San Francisco, CA, USA, 2017, pp. 1–6.

[24] F. Zafar, D. Karunatilaka, and R. Parthiban, "Dimming schemes for visible light communication: The state of research," *IEEE Wireless Commun.*, vol. 22, no. 2, pp. 29–35, Apr. 2015.

[25] H. Elgala and T. D. C. Little, "Reverse polarity optical-OFDM (RPO-OFDM): Dimming compatible OFDM for gigabit VLC links," *Opt. Exp.*, vol. 21, no. 20, pp. 24288–24299, Oct. 2013. [Online]. Available: http://www.opticsexpress.org/abstract.cfm?URI=oe-21-20-24288

[26] T. Q. Wang and X. Huang, "Fractional reverse polarity optical OFDM for high speed dimmable visible light communications," *IEEE Trans. Commun.*, vol. 66, no. 4, pp. 1565–1578, Apr. 2018.

[27] Y. Sun, F. Yang, and J. Gao, "Novel dimmable visible light communication approach based on hybrid LACO-OFDM," *J. Lightw. Technol.*, vol. 36, no. 20, pp. 4942–4951, Oct. 15, 2018.

[28] G. Ntogari, T. Kamalakis, J. W. Walewski, and T. Sphicopoulos, "Combining illumination dimming based on pulse-width modulation with visible-light communications based on discrete multitone," *J. Opt. Commun. Netw.*, vol. 3, no. 1, pp. 56–65, Jan. 2011. [Online]. Available: http://jocn.osa.org/abstract.cfm?URI=jocn-3-1-56

[29] N. Serafimovski *et al.*, "Practical implementation of spatial modulation," *IEEE Trans. Veh. Technol.*, vol. 62, no. 9, pp. 4511–4523, Nov. 2013.

[30] S. Gokceli, E. Basar, M. Wen, and G. K. Kurt, "Practical implementation of index modulation-based waveforms," *IEEE Access*, vol. 5, pp. 25463–25473, 2017.

[31] N. Robertson. (2019). *Compute Modulation Error Ratio(MER) for QAM*. [Online]. Available: https://www.dsprelated.com/showarticle/1305.php
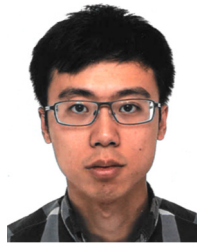
Cheng Chen received the B.Eng. degree in electronic and electrical engineering from the University of Strathclyde, Glasgow, U.K., in 2011, the M.Sc. degree in communications and signal processing from the Imperial College, London, U.K., in 2012, and the Ph.D. degree in electrical engineering from the University of Edinburgh, Edinburgh, U.K., in 2017. He is currently employed as a Research Associate with the Li-Fi Research and Development Centre, The University of Strathclyde and is working in the field of visible light communications and LiFi networks. His main research interests are in the areas of optical wireless communication, visible light communication, and wireless communication for 6G. He has authored or coauthored 30 publications in these areas.

Trang Nguyen received the Biomedical Engineering degree from the Hanoi University of Science and Technology, Vietnam, in 2013, and the M.Sc. and Ph.D. degrees in electrical and electronics engineering from Kookmin University, South Korea, in 2015 and 2018, respectively. He is a currently a Research Associate with LiFi Research and Development Center, The University of Strathclyde. His research interests mainly focus on the physical layer of optical wireless communications. He had been an active Member and a voting Member of IEEE 80.15.7m Task Group within IEEE standards association from 2015 to 2018.

Mohamed Sufyan Islim received the M.Sc. (Distinction) degree in communications engineering from Aleppo University, Syria, in 2013, and the M.Sc. degree in signal processing and communications and the Ph.D. degree in digital communications from The University of Edinburgh, U.K. in 2014 and 2019, respectively. He is currently a Postdoctoral Research Associate with the LiFi Research and Development Centre, University of Strathclyde. He has coauthored 11 conference papers, 14 journal papers, two book chapters, and two pending patents. His main research interests include optical OFDM, LiFi, and optical wireless communications. He was awarded the Global Edinburgh Syrian Scholarship from Edinburgh University in 2013. He received the IEEE Communications Chapter Prize for the Best M.Sc. Project in 2014.

Harald Haas (Fellow, IEEE) received the Ph.D. degree from The University of Edinburgh in 2001. He is a Distinguished Professor of Mobile Communications with The University of Strathclyde and the Director of the LiFi Research and Development Centre. He also set-up and Co-Founded pureLiFi Ltd., which it currently serves as a Chief Scientific Officer. He has authored over 550 conference and journal papers. His main research interests are in optical wireless communications, hybrid optical wireless and RF communications, spatial modulation, and interference coordination in wireless networks. His team invented spatial modulation. In 2016, he received the Outstanding Achievement Award from the International Solid State Lighting Alliance. In 2019, he was a recipient of IEEE Vehicular Society James Evans Avant Garde Award. He introduced LiFi to the public at an invited TED Global talk in 2011. LiFi was listed among the 50 best inventions in TIME Magazine in 2011. He gave a second TED Global lecture in 2015 on the use of solar cells as LiFi data detectors and energy harvesters. He received a Royal Society Wolfson Research Merit Award in 2017 and was elevated to IEEE Fellow. In 2018, he received a three-year EPSRC Established Career Fellowship extension and was Elected Fellow of the IET. He was elected a Fellow of the Royal Society of Edinburgh in 2017. He was an Elected Fellow of the Royal Academy of Engineering in 2019.